

Comparative XRD Analysis of the Stress State of a Thin Tungsten Ribbon and Magnetron-Sputtered Tungsten Coatings

S.N. Danilchenko*, A.V. Kochenko, A.N. Kalinkevich, O.Yu. Karpenko, V.A. Baturin

Institute of Applied Physics NASU, 58, Petropavlivska St., 40000 Sumy, Ukraine

(Received 12 April 2021; revised manuscript received 23 February 2022; published online 28 February 2022)

The stress state of a thin tungsten ribbon and magnetron-sputtered tungsten coatings on a ferrite steel substrate were investigated by X-ray tensometry ($\sin^2\psi$ method). In-plane biaxial compressive stresses were revealed in the samples of the tungsten ribbon: $\sigma_y = -0.40$ GPa and -0.45 GPa in the rolling direction and $\sigma_x = -0.28$ GPa and -0.25 GPa in the direction perpendicular to the rolling direction from the front and back sides, respectively. The magnetron-sputtered tungsten coatings have in-plane equiaxial stresses, rotationally symmetric with respect to the surface normal ($\sigma_x = \sigma_y = \sigma_\phi$). The stress magnitudes in the tungsten coatings are several times higher than those in the tungsten ribbon. The highest compressive stress (-3.7 GPa) was found in a tungsten coating with a nominal thickness of 250 nm, in a coating with a thickness of 460 nm, the stress level was 1.5 times lower. The peculiarity of the analysis was that in the case of the tungsten ribbon, the line (310) was used, which certainly belongs to the precision region of the diffraction angles, while in the case of the tungsten coatings, due to the overlap of (310) α -W and (220) α -Fe lines, the lines (220) and (211) were used, which satisfy this condition to a lesser extent. The use of relatively soft Co-radiation (compared to Cu-radiation) somewhat mitigated this discrepancy. The stress-free lattice parameter (a_0), corresponding to the undeformed cross section of the strain ellipsoid, was lower in the tungsten ribbon and higher in the coatings than the reference value for α -W; as the coating thickness increases, this difference increases. The reasons for these differences are discussed. Considering the broadening of the tungsten diffraction peaks, it was found that both the small size of the crystallites and the microstrain of the crystal lattice are the cause of this broadening in the samples of both groups, although the microstructure of the coatings is much more defective.

Keywords: X-ray diffraction, Tungsten, Steel, Coating, X-ray tensometry, Residual stresses, Lattice parameter, Line broadening.

DOI: [10.21272/jnep.14\(1\).01026](https://doi.org/10.21272/jnep.14(1).01026)

PACS numbers: 61.05.cp, 07.10.Lw

1. INTRODUCTION

Tungsten (W), due to such properties as a high melting point, low physical sputtering yield, and low solubility of hydrogen isotopes, is one of the candidate materials for plasma-facing elements of thermonuclear reactors [1, 2]. Typically, tungsten is used for reactor components, either in the form of coatings or bulk lamellas. Also in high-energy equipment, tungsten is very often used in the form of a rolled tape or foil. It is natural to expect that tungsten elements fabricated by different methods (rolling, forging, sputtering, etc.) can have different surface stress states.

Residual and formed during operation mechanical stresses on the surface of structural elements of high-energy systems significantly affect their service properties and, ultimately, the resource. It is known that the initial residual stresses have a strong influence on surface cracking, and unstressed surfaces are more resistant to cracking [3, 4]. Numerous simulation experiments have shown that the initial stress state of the surface of tungsten-based materials can vary greatly under thermal and radiation loads [2-5].

In studies of the stress state of the surface of metal materials and strain effect in them, the methods of X-ray tensometry [3, 6-8] and tensorometry [9, 10] are widely used. In crystalline materials, interplanar spacings (d_{hkl}) can serve as an in-situ strain gauge that can be measured by X-ray diffraction. Elastic strain and stress can be calculated using the change in d -

spacing of the stressed sample from its stress-free state. The accuracy of stress determination by these methods for steels and hard alloys lies within 40-110 MPa [11].

The aim of this study was to compare the stress state of a rolled thin tungsten ribbon and magnetron-sputtered tungsten coatings on steel substrates, in which the ribbon was used as a sputtered target. The task was complicated by the fact that the X-ray diffraction patterns of the samples of tungsten coatings contained, along with the lines of tungsten, the lines of the steel substrate. Because of this, when determining the residual stresses of thin tungsten ribbon and tungsten coatings, different reflections (hkl) were used.

2. MATERIALS AND METHODS

An unannealed tungsten ribbon (0.2 mm thick) with a W content of 99.95 wt. % (TU 48-19-106-91) was taken as the starting material for research. For XRD examination, flat samples of 10×12 mm were cut out. The surface of the samples was thoroughly cleaned with an ethanol solution.

Tungsten coatings were deposited on steel substrates by the method of high-frequency magnetron sputtering. The deposition was carried out at a high frequency discharge power of ~ 200 W at a frequency of 13.5 MHz in an argon medium. The argon pressure was maintained within 1 Pa. As a target, a disk 80 mm in diameter was fabricated from the tungsten ribbon. The rotating substrate holder was used. The target-

* danilserg50@gmail.com

substrate distance was chosen in such a way as to minimize the effect of substrate heating during tungsten sputtering.

The coatings were deposited without heating the substrate. The steel substrate was preliminarily polished to a “mirror” state. The thickness of the deposited W coating was estimated by optical interferometry (MII-4 Linnik microinterferometer, LOMO, St. Petersburg, Russia) and was 460 nm and 250 nm (hereafter “thick” and “thin” coatings).

The structural characteristics of the samples were studied by X-ray diffraction using a DRON-4-07 instrument (“Burevestnik”) connected to the computer-aided experiment control and data processing system. DifWin-1 software package (Etalon PTC Ltd, Russia) was used for registration of diffractograms and their primary processing. We used $\text{CoK}\alpha$ radiation (relatively soft compared to traditional copper radiation, $\lambda_{\text{CoK}\alpha} = 0.179$ nm) in order to bring the positions of analytical lines with small hkl closer to the precision range of diffraction angles ($\theta = 55\text{--}70^\circ$). The profiles of the analyzed lines were recorded with a 0.25 mm tube slit, without Soller slits, and without sample rotation.

To evaluate the residual stresses, we applied the so-called $\sin^2\psi$ method: measurement of angle-dependent lattice strains by tilting the sample along the axis perpendicular to the beam-detector axis (in Fig. 1, Ψ is the tilt angle). This method is based on the ratio below, which is a consequence of Hooke's law [3, 6, 8]:

$$\frac{d_{\psi,\varphi}^{hkl} - d_0^{hkl}}{d_0^{hkl}} = \frac{1+\nu}{E} \sin^2\psi \cdot \sigma_\varphi + \frac{d_{\perp}^{hkl} - d_0^{hkl}}{d_0^{hkl}}, \quad (1)$$

where σ_φ is the in-plane stress associated with the azimuthal direction φ (Fig. 1), E is the Young modulus

and ν is the Poisson ratio, $\frac{d_{\perp}^{hkl} - d_0^{hkl}}{d_0^{hkl}} = \varepsilon_{\perp} = \varepsilon_{\perp}$ is the

lattice strain in the direction perpendicular to the sample surface (for $\Psi=0$), $\frac{d_{\psi,\varphi}^{hkl} - d_0^{hkl}}{d_0^{hkl}} = \varepsilon_{\psi,\varphi}$ is the lattice

strain in an arbitrary direction specified by the angles Ψ and φ , d_0^{hkl} is the d -spacing of the hkl plane in the stress-free state.

By XRD measurement of the lattice spacing for a range of available tilt angles, one can construct the d - $\sin^2\Psi$ plot, extrapolation of which up to $\Psi=90^\circ$ gives the in-plane strain and therefore stress in the x or y direction (σ_x or σ_y) depending on the angle φ (Fig. 1).

In this work, for α -W cubic lattice, assuming $\varepsilon_{\perp} = 0$ on the sample surface, the values of strain (ε_φ) and stress (σ_φ) associated with an arbitrary in-plane azimuthal direction were calculated by the formulas:

$$\varepsilon_\varphi = \frac{a_\varphi - a_0}{a_0}, \quad (2)$$

$$\sigma_\varphi = \frac{1}{1-\nu} \cdot \varepsilon_\varphi \cdot E, \quad (3)$$

where a_φ is the tungsten lattice spacing at $\sin^2\Psi=1$ ($\Psi=90^\circ$) obtained from the extrapolation of the a - $\sin^2\Psi$

plot; a_0 is the value of the W lattice spacing in an unstressed section defined from the a - $\sin^2\Psi$ graph at $\sin^2\Psi_0 = (2\nu/(1+\nu)) = 0.4615$; $\nu = 0.3$ and $E = 400$ GPa are the values of α -W bulk elastic constants, taken in the first approximation, under the assumption of mechanical isotropy [4, 5].

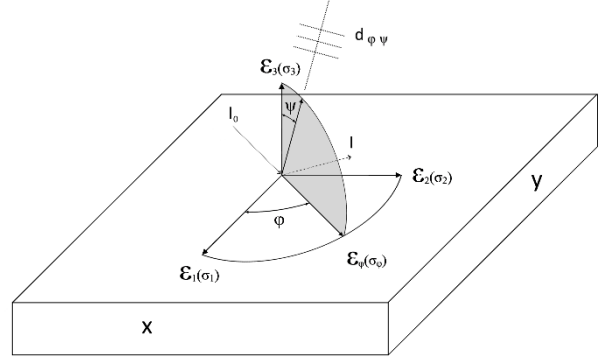


Fig. 1 – Schematic representation of X-ray geometry for the $\sin^2\psi$ method

It should be taken into account that the number of points on the $\sin^2\psi$ plot is limited by the condition $\theta_{hkl} > \Psi$ so that the angle of incidence of the primary beam $\alpha = \theta_{hkl} - \Psi$ remains positive. Then, when using lines with relatively small hkl for analysis, “softer” (long-wavelength) radiation should be used to increase θ_{hkl} .

In our work, for each sample, X-ray tensometry analysis was performed in several azimuthal directions, i.e., sequentially after turning the sample around the axis perpendicular to the surface by 90° for the ribbon and by 45° for coatings.

On the steel surface, which served as a substrate for W coatings, residual stresses were not detected or were at the level of the method error.

3. RESULTS AND DISCUSSION

Fig. 2 shows that the diffraction pattern of a thin tungsten ribbon corresponds to the α -W (body-centered cubic lattice) JCPDS 04-806 card. The pattern demonstrates the presence of a pronounced cubic texture, the crystallites principally lie in a cube plane $\{001\}$ parallel to the sheet plane.

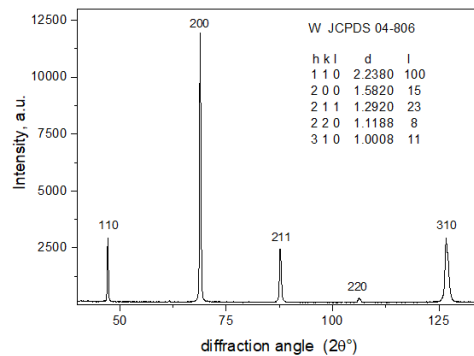


Fig. 2 – X-ray diffraction pattern of a thin tungsten ribbon demonstrating a strong texture

As revealed, the texture intensity is almost the same on the front and back sides of the tungsten ribbon. For the tungsten ribbon, the (310) line was used in further analysis to get the tungsten lattice spacing in the range of tilt angle ψ , and then to evaluate the magnitude and direction of stresses. Note that the (310) line is located in the high-precision diffraction region for cobalt radiation ($\theta_{310} = 63^\circ$).

X-ray diffraction patterns of two samples of steel with W coatings of different thicknesses and uncoated steel are shown in Fig. 3. As can be seen, the phase composition of the steel corresponds to α -Fe (ferrite, body-centered cubic lattice, JCPDS 06-698), and the W coating corresponds to the JCPDS 04-806 card. In the diffraction patterns of W coatings, the distribution of intensity over reflections indicates the presence of a texture in which crystallographic planes of the $\{hh0\}$ type are predominantly located parallel to the surface. It is assumed that the observed texture is an axial-type texture (fiber texture), which is typical of polycrystalline thin films and coatings created by physical vapor deposition [6, 10]. The (310) tungsten line overlaps with the (220) iron line, which makes it impossible to analyze macrostresses in coatings using this line. The (220) ($\theta_{220} = 52.6^\circ$) and (211) ($\theta_{211} = 43.5^\circ$) tungsten lines remain suitable for analysis, although they can be attributed to a lesser extent than the (310) line to the precision region of diffraction angles. In addition, in the case of a "thin" coating, the analysis of macrostresses using the (220) line is fraught with serious inaccuracy due to its low intensity. In view of these circumstances, only the (211) line, approached to high-precision region, was used to analyze the macrostresses in both coatings, and the (220) line was additionally used for a "thick" coating. This provided an opportunity to compare the stress magnitude calculated for the same coating using different lines.

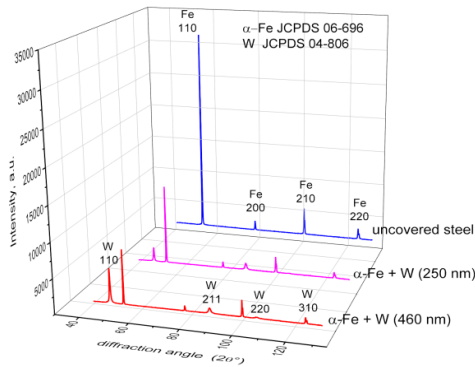


Fig. 3 – X-ray diffraction patterns of an uncoated steel substrate and the same steel with tungsten coatings 250 nm and 460 nm thick

Residual stresses in the tungsten ribbon were determined in two directions: in the sheet rolling direction and in the perpendicular direction. In the first case, when examining, the sample was located with the rolling direction parallel to the beam-detector axis, in the second case, with the rolling direction perpendicular to the beam-detector axis. In-plane compressive strains, which in turn imply in-plane compressive stresses, were found in both directions, but they are

appreciably higher for the sheet rolling direction (Fig. 4, Table 1). As can be seen, despite the fact that compressive stresses act during rolling on the entire surface of the tungsten sheet, however, in the sheet rolling direction, the material acquires slightly higher residual stresses than in the direction perpendicular to the rolling direction.

Table 1 – Experimental data processing results for the rolled thin tungsten ribbon

Characterization of the specimen	Front side, sheet rolling direction	Front side, perpendicular to the rolling direction	Back side, sheet rolling direction	Back side, perpendicular to the rolling direction
XRD line	310	310	310	310
a_\perp , nm	0.31651	0.31649	0.31653	0.31652
a_0 , nm	0.31632	0.31636	0.31632	0.31640
a_ϕ , nm	0.31610	0.31620	0.31607	0.31626
$\varepsilon_\phi \cdot 10^3$	-0.70	-0.50	-0.79	-0.45
σ_ϕ , MPa	-401.0	-283.6	-449.8	-254.6

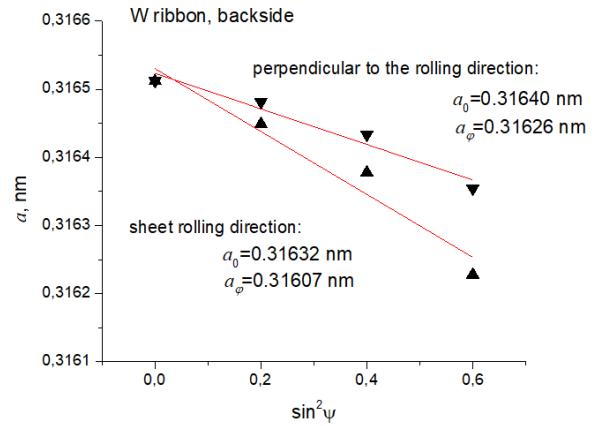


Fig. 4 – a - $\sin^2 \psi$ plots and associated linear regressions for the sample of the tungsten ribbon; up-vertex triangles correspond to the sheet rolling direction, down-vertex triangles correspond to the direction perpendicular to the rolling direction

The front and back sides of the tungsten ribbon were analyzed in the same way, and the results revealed that the macrostress state on both sides of the sheet is identical (Table 1).

The stress-free lattice parameter a_0 for both sides and both directions of the rolled thin tungsten ribbon is determined to be smaller than the bulk reference parameter (0.31632 ± 0.31640 nm vs 0.31652 nm), indicating lattice contraction. The most probable reason is the presence of a solid solution of vacancies that enter the volume during severe plastic deformation at the rolling. It is characteristic that the smallest values of a_0 correspond to the highest values of macrostrains and macrostresses for the sheet rolling direction, while for the direction perpendicular to the rolling direction, on the contrary, the obtained values of a_0 are somewhat larger at lower macrostrains.

In the magnetron-sputtered tungsten coatings, significant compressive macrostresses were revealed (see Fig. 5, Table 2), which are several times higher than those on the surface of the thin tungsten ribbon. As expected, the magnetron-sputtered tungsten coatings

have in-plane equiaxial stresses, rotationally symmetric with respect to the surface normal ($\sigma_x = \sigma_y = \sigma_\varphi$).

In contrast to the rolled tungsten ribbon, for the sputtered tungsten coatings, all calculated stress-free lattice parameters are larger than the bulk reference parameter (0.31668±0.31746 nm vs 0.31652 nm), indicating lattice expansion.

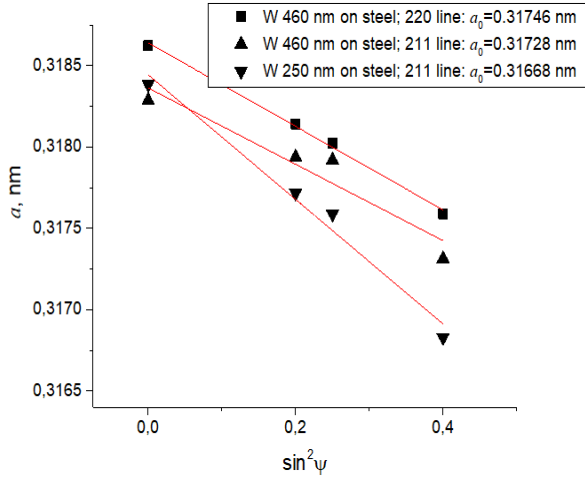


Fig. 5 – a - $\sin^2 \Psi$ plots and associated linear regressions for the samples of magnetron sputtered tungsten coatings; note that in the case of copper radiation, it will not be possible to obtain the point $\sin^2 \Psi = 0.4$ on the a_{211} - $\sin^2 \Psi$ graph, because in this case $\theta_{211} < \Psi$ and $a < 0$

Table 2 – Experimental data processing results for the magnetron sputtered tungsten coatings

Thickness of the coatings	460 nm		250 nm	
	XRD line	220	211	211
a_{\perp} , nm		0.31864	0.31836	0.31844
a_0 , nm		0.31746	0.31728	0.31668
a_{φ} , nm		0.31608	0.31602	0.31462
$\varepsilon_{\varphi} \cdot 10^3$		- 4.35	- 3.97	- 6.51
σ_{φ} , MPa		- 2485.7	- 2271.0	- 3717.0

Moreover, for a “thick” coating, this difference is greater than for a “thin” one, while macrostresses are much greater for a “thin” coating than for a “thick” one. This can be explained by the fact that high-energy tungsten atoms and working gas ions are introduced into interstitial positions during coating deposition, and these insertions into the lattice increase with increasing coating thickness (time of magnetron sputtering). This increase in the number of interstitial complexes is consistent with a slight increase in the lattice parameter.

It should be noted a slight difference in the values of macrostresses ($< 10\%$), determined using the lines (211) and (220) in the “thick” coating, which can be explained by the influence of experimental factors: analysis using the (211) line is associated with larger errors. At the same time, the macrostresses determined using the (211) line for two coating samples of different thicknesses differ to a much greater extent ($\geq 50\%$), which indicates the qualitative significance of this difference.

From the analysis of the physical broadening of the diffraction peaks of tungsten, it follows that both the small size of crystallites and the microstrain of the crystal lattice are the cause of this broadening in the samples of both groups. This is confirmed by the fact that for all samples the physical broadening of the lines (110) and (220), β_1 and β_2 , respectively, satisfies the condition: $\cos \theta_1 / \cos \theta_2 < \beta_2 / \beta_1 < \tan \theta_2 / \tan \theta_1$ [9]. It is characteristic that the peaks of W coatings are broader than those of the tungsten ribbon, and with increasing θ the physical broadening grows faster. This indicates that the coatings have large microstresses and smaller crystallite sizes, i.e., their microstructure is more defective than that of the tungsten ribbon.

Based on the presented results, we suggest that the magnetron-sputtered tungsten coatings are a good model for investigating the effect of residual stresses on hydrogen permeation into tungsten. By creating tungsten coatings of different thicknesses and having different stress states, one can establish some critical aspects of hydrogen permeability of mechanically loaded tungsten-based elements and constructions, which is of great importance for fusion power engineering. In this case, X-ray tensometry methods should be combined with gas permeation experimental techniques [11]. The attractiveness of this approach is that magnetron-sputtered coatings can be deposited on a great variety of substrates (metals, ceramics or even biopolymers [12-14]). This provides an opportunity to create stress states in the coatings without applying real mechanical loading.

4. CONCLUSIONS

In this work, using X-ray tensometry, a significant difference in the magnitude of residual stresses on the surface of a rolled tungsten ribbon and magnetron-sputtered thin tungsten coatings on ferritic steel was shown. The compressive stresses of the tungsten ribbon in the rolling direction and in the perpendicular direction have significant differences, i.e., during rolling, the material acquires slightly greater residual stresses precisely in the rolling direction than in the perpendicular one. In the tungsten coatings on a steel substrate, equiaxial compressive stresses, axisymmetric with respect to the surface normal, were found, the absolute values of which are several times higher than those in the rolled tungsten ribbon. With an increase in the coating thickness from 250 to 460 nm, the level of macrostresses decreased by about 1.5 times. It has been suggested that tungsten coatings can serve as a model for studying the dependence of hydrogen permeability on the surface stress state, which is important for assessing the reliability of mechanically loaded elements and structures based on tungsten for fusion power engineering.

ACKNOWLEDGEMENTS

This work was partly supported by JAEA (Research Contract No. 24191), as a part of Coordinated Research Project F43025, and partly supported by the National Academy of Sciences of Ukraine (state registration number of the work 0120U105445).

REFERENCES

1. T. Hirai, S. Panayotis, V. Barabash, C. Amzallagh, F. Escourbiac, A. Durocher, M. Merola, J. Linke, Th. Loewenhoff, G. Pintsuk, M. Wirtz, I. Uytendhouwend, *Nuclear Mater. Energy* **9**, 616 (2016).
2. I.E. Garkusha, S.V. Malykhin, V.A. Makhlai, A.T. Pugachev, S.V. Bazdyrieva, N.N. Aksenov, *Tech. Phys.* **59** No 11, 1620 (2014).
3. S.V. Malykhin, I.E. Garkusha, V.A. Makhlai, S.V. Surovitskiy, S.S. Herashchenko, O.I. Girka, *Nucl. Instrum. Methods Phys. Res. B: Beam Interact. Mater. At.* **481**, 6 (2020).
4. V.A. Makhlai, I.E. Garkusha, J. Linke, S.V. Malykhin, N.N. Aksenov, O.V. Byrka, S.S. Herashchenko, S.V. Surovitskiy, M. Wirtz, *Nuclear Mater. Energy* **9**, 116 (2016).
5. S.V. Malykhin, S.V. Surovitskiy, V.A. Makhlai, N.N. Aksenov, O.V. Byrka, S.S. Borisova, S.S. Herashchenko, V.V. Reshetnyak, *Probl. At. Sci. Technol.* **1**, 123 (2017).
6. F. Motazedian, Zh. Wu, J. Zhang, B. S. Shariat, D. Jiang, M. Martyniuk, Y. Liu, H. Yang, *Mater. Design* **181**, 108063 (2019).
7. T.J. Vink, W. Walrave, J.L.C. Daams, A.G. Dirks, M.A.J. Somers, K.J.A. Van den Aker, *J. Appl. Phys.* **74** No 2, 988 (1993).
8. B. Girault, D. Eyidi, P. Goudeau, T. Sauvage, P. Guérin, E.L. Bourhis, P.O. Renault, *J. Appl. Phys.* **113** No 17, 174310 (2013).
9. Y.S. Umansky, Y.A. Skakov, A.I. Ivanov, L.N. Rastorguev, *Crystallography, X-Ray Diffraction and Electron Microscopy* (Moscow: Metallurgiya: 1982) (in Russian).
10. B. Girault, P. Villain, E. Le Bourhis, P. Goudeau, P.O. Renault, *Surf. Coat. Technol.* **201** No 7, 4372 (2006).
11. M. Mouanga, P. Berçot, J. Takadoum, *Corrosion Sci.* **52** No 6, 2010 (2010).
12. K.V. Tyshchenko, L.V. Odnodvoret, I.Yu. Protsenko, *Metallofizika i Noveishie Tekhnologii* **33** No 10, 1351 (2011).
13. S.I. Protsenko, L.V. Odnodvoret, I.Y. Protsenko, *Springer Proceedings in Physics* **156**, 345 (2015).
14. O.V. Kalinkevich, O.Yu. Karpenko, Ya.V. Trofimenko, A.M. Sklyar, V.Yu. Illiashenko, A.N. Kalinkevich, V.A. Baturin, S.N. Danilchenko, *Chem. Phys. Technol. Surf.* **8**, 410 (2017).

Порівняльний рентген-дифракційний аналіз напруженого стану вольфрамової тонкої стрічки та магнетронно напилених вольфрамових покриттів

С.М. Данильченко, О.В. Коченко, О.М. Калінкевич, О.Ю. Карпенко, В.А. Батурін

Інститут прикладної фізики НАНУ, вул. Петропавлівська, 58, 40000 Суми, Україна

Методом рентгенівської тензометрії ($\sin^2\psi$ метод) досліджено напружений стан прокатої вольфрамової стрічки та покриттів вольфраму, магнетронно напилених на підкладці з феритної сталі. У вольфрамовій стрічці виявлені площинні двовісні стискаючі напруження $\sigma_y = -0,40$ ГПа і $-0,45$ ГПа у напрямку прокатки та $\sigma_x = -0,28$ ГПа і $-0,25$ ГПа у напрямку, перпендикулярному напрямку прокатки з лицьової та зворотної сторони, відповідно. У покриттях вольфраму на сталевій підкладці виявлені площинні рівновісні стискаючі напруження, осесиметричні відносно нормалі до поверхні ($\sigma_x = \sigma_y = \sigma_\phi$). Величини напружень у вольфрамових покриттях у кілька разів вищі, ніж у вольфрамовій стрічці. Найбільше напруження стиснення ($-3,7$ ГПа) виявлено у вольфрамовому покритті номінальною товщиною 250 нм, у покритті товщиною 460 нм рівень напружень у 1,5 рази нижчий. Особливістю проведеного аналізу було те, що у випадку вольфрамової стрічки використовувалася лінія (310), яка безумовно належить до прецизійної області кутів дифракції, тоді як у випадку вольфрамових покриттів через перекриття (310) лінії W та лінії (220) α -Fe підкладки, використано лінії (220) та (211), які задовольняють цій умові меншою мірою. Застосування відносно м'якого Со-випромінювання (у порівнянні з Си-випромінюванням) дещо пом'якшило цю невідповідність. Параметр ґратки, що відповідає недеформованому перетину еліпсоїда деформації (a_0), у вольфрамовій стрічці був нижчим, а у покриттях – вищим ніж довідкове значення для α -W; зі збільшенням товщини покриття ця відмінність збільшується. Причини цих розбіжностей обговорено. З розгляду розширення дифракційних піків вольфраму встановлено, що як малі розміри кристалітів, так і мікродеформації кристалічної ґратки є причиною цього розширення в зразках обох груп, хоча мікроструктура покриттів значно дефектніша.

Ключові слова: Рентгенівська дифракція, Вольфрам, Сталь, Покриття, Рентгенівська тензометрія, Макронапруження, Параметр решітки, Розширення ліній.